Genetically Engineered Metal Ion Binding Sites on the Outside of a Channel's Transmembrane β-Barrel

John J. Kasianowicz,* Daniel L. Burden,# Linda C. Han,* Stephen Cheley,§ and Hagan Bayley§

*National Institute of Standards and Technology, Biotechnology Division, Gaithersburg, Maryland 20899; #Indiana University, Department of Chemistry, Bloomington, Indiana 47405; and §Department of Medical Biochemistry and Genetics, Texas A & M University, Health Science Center, College Station, Texas 77843-1114 USA

ABSTRACT We are exploring the ability of genetically engineered versions of the *Staphylococcus aureus* α-hemolysin (αHL) ion channel to serve as rationally designed sensor components for analytes including divalent cations. We show here that neither the hemolytic activity nor the single channel current of wild-type αHL was affected by [Zn(II)] $\leq$ 1 mM. Binding sites for the divalent cations were formed by altering the number and location of coordinating side chains, e.g., histidines and aspartic acids, between positions 126 and 134, inclusive. Several mutant αHLs exhibited Zn(II)-induced current noise that varied with Zn(II) concentration. At a fixed divalent cation concentration, the current fluctuation kinetics depended on the analyte type, e.g., Zn(II), Cu(II), Ni(II), and Co(II). We also show that the ability of Zn(II) to change the mutant channel current suggests that the pore's topology is β-sheet and that position 130 is near the turn at the *trans* mouth. Both conclusions are consistent with the crystal structure of WT-αHL oligomerized in detergent. Our results, in the context of the channel's crystal structure, suggest that conductance blockades were caused by Zn(II) binding to the outside surface of the pore. Thus, analyte-induced current blockades alone might not establish whether an analyte binding site is inside a pore.

INTRODUCTION

Protein ion channels perform a wide variety of functions in cells. By virtue of their ability to respond to various inputs, including the concentration of specific analytes (e.g., neurotransmitters; Hille, 1992), channels might prove useful as sensors for water-soluble compounds. This could be accomplished by placing binding sites for the analyte of choice in the channel's pore. If the analyte bound reversibly to the site(s) and caused a well-defined conductance change, its concentration could be inferred from the mean conductance of a fixed number of channels or from the mean time a single channel spends in the analyte-bound conductance state.

In an effort to rationally design and construct sensors for specific chemicals in solution, we are genetically engineering various types of analyte binding sites into the channel formed by *Staphylococcus aureus* α-hemolysin (αHL) (Walker et al., 1994; Kasianowicz et al., 1994; Braha et al., 1997). α-Hemolysin has several characteristics that make it particularly attractive for this purpose. Although the 293-residue monomer (Gray and Kehoe, 1984; Walker et al., 1992) is water-soluble, it binds spontaneously to a variety of lipid membranes, and self-assembles to form heptameric pores from identical monomers (Gouaux et al. 1994; Song et al., 1996). Since the experimentally determined narrowest segment of the channel's pore diameter is ~2 nm (Krasilnikov et al., 1992; Korchev et al., 1995; Kasianowicz et al., 1996; Bezrukov et al., 1996; Song et al., 1996; Bezrukov and Kasianowicz, 1997), the pore is large enough to accommodate engineered analyte binding sites. However, the pore is sufficiently small that the binding of an analyte to a receptor site inside the pore will cause marked changes in the channel's current. In addition, unlike many voltage-gated channels, the αHL channel remains in the fully open state for long periods of time (Kasianowicz et al., 1996).

Wild-type αHL (WT-αHL) has been shown to sense different ions in solution and to determine their concentration. For example, the reversible binding of hydrogen or deuterium ions to the channel causes rapid current fluctuations (Bezrukov and Kasianowicz, 1993; Kasianowicz and Bezrukov, 1995). The pH dependence of the current spectral density allowed the determination of the rate constants and the equilibrium constants for these reactions as well. Those studies provided the analytical basis for the use of the αHL channel in sensing applications.

We previously demonstrated that αHL can be genetically engineered to detect transition metal divalent cations. The current carried by the mutant αHL-H5, in which five consecutive amino acids in a glycine rich region of the protein (residues 130–134, inclusive) were replaced with histidines, was markedly blocked by the addition of 100 μM Zn(II) added to either side of the membrane (Walker et al., 1994; Kasianowicz et al., 1994). The work reported here extends those studies, identifies several residues that are near one mouth of the pore, and suggests that the pore's secondary structural motif is β-sheet. These results are in good agreement with the recently determined crystal structure of WT-αHL oligomerized in detergent (Song et al., 1996).

Received for publication 26 February 1998 and in final form 15 October 1998.

Address reprint requests to Dr. John J. Kasianowicz, Biotechnology Division, National Institute of Standards and Technology, Gaithersburg, MD 20899-8311. Tel.: 301-975-5853; Fax: 301-330-3447; E-mail: john.kasianowicz@nist.gov.

Daniel L. Burden's current address is NIST, Biotechnology Division, Gaithersburg, MD 20899.

0006-3495/99/02/837/09 $2.00

METHODS

Modified region of the primary sequence

Table 1 illustrates the segment of the WT-αHL primary structure that was modified to include binding sites for divalent cations and illustrates the notation used herein to describe the mutations.

Protein Expression, Purification, and Assay

Histidine scanning mutagenesis

Six histidine mutants of αHL encompassing residues 129–134 were made following the method of Kunkel (1985) using pT7-NPH8S(K8A) as the template (Walker et al., 1992). This plasmid encodes the protease-resistant αHL mutant K8A (Walker et al., 1992). The following sense primers (5′ → 3′) were used for the mutagenesis. Ionizable residues are underlined and nucleotides that differ from WT-αHL DNA are represented in lowercase lettering.

T129H GTTACTGGTGATGATcatGGAAAAATTGGgGGCCTTATTGGTG,

G130H CTGGTGATGATACAcatAAAATTGGgGGCCTTATTGGTG,

K131H GTGATGATACAGGAcatATTGGgGGCCTTATTGGTG,

I132H GATGATACAGGAAAAcatGGgGGCCTTATTGGTG,

G133H GATACAGGAAAAATTcatGGCCTTATTGGTG,

G134H CAGGAAAAATTGGCcatCTTATTGTGCAAATG.

Mutants were screened by agarose gel analysis of *Aci*I-digested plasmid isolates (WT-αHL DNA is cleaved by *Aci*I while the mutant DNAs are not). Mutations were verified by sequencing through the altered region and mutant G130H was sequenced in its entirety. No sequence differences were observed in αHL-DNA other than those present in the mutagenic oligonucleotides.

Cassette mutagenesis

For further mutagenesis of the DNA encoding the central region of the αHL polypeptide, eight restriction endonuclease sites (*Hpa*I, *Bsi*WI, *Bst*EII, *Spe*I, *Stu*I, *Apa*I, *Avr*II, and *Afl*II) were introduced into pT7-NPH8S (K8A). These sites do not occur elsewhere in the vector or insert. Four of these sites (*Hpa*I, *Bsi*WI, *Bst*EII, and *Afl*II), representing sequences between amino acid residues 114 and 148, were introduced by PCR of 5′ and 3′ segments of the αHL gene using the following primers: HB203 (5′ half; sense primer) CGGGATCCTAATACGACTCACTATAGGG, HB497 (5′ half; antisense primer) CCAGTAAGGTTACCGTTGAATCCGTACGTTAACGTACTCATATACTC, HB498 (3′ half; sense primer) GGTGCAAAGGTAACCCTAGGTCATACACTTAAGTATGTTCAACC, HB172 (3′ half; antisense primer) AAACATCATTTCTGAAGCTTTCGGCTAAAG. The PCR product representing the 5′ segment of the αHL gene was digested with *Nde*I and *Bst*EII and that representing the 3′ segment with *Bst*EII and *Hin*dIII. Subsequent three-way ligation with the vector PT7-SMC (digested with *Nde*I and *Hin*dIII (Cheley et al., 1997)) yielded an αHL construct with a deletion in the central region, which was then digested with *Bst*EII and *Afl*II. Ligation of the digested vector to an oligonucleotide cassette flanked by the same sites resulted in a full-length re-engineered αHL. The following oligonucleotides were used to generate the double-stranded synthetic cassette: HB499 (upper strand) GTAACCTTACTGGTGATGATACTAGTAAAATTGGAGGCCTTATTGGGGCCCAGGTTTCCCTAGGTCATACAC, HB500 (lower strand) TTAAGTGTATGACCTAGGGAAACCTGGGCCCCAATAAGGCCTCCAATTTTACTAGTATCATCACCAGTAAG. DNA sequencing of the entire re-engineered αHL gene revealed two base deletions and one base substitution in the synthetic insert. These errors were repaired by replacing the DNA between *Bst*EII and *Stu*I sites with a synthetic oligonucleotide: HB521 (upper strand) GTAACCTTACTGGTGATGATACTAGTAAAATTGGAGG, HB522 (lower strand) CCTCCAATTTTACTAGTATCATCACCAGTAAG. The corrections were confirmed by DNA sequencing. Of the eight new restriction endonuclease sites, four (*Bst*EII, *Spe*I, *Apa*I, and *Avr*II) resulted in conservative amino acid replacements (V124L, G130S, N139Q, I142L) and four (*Hpa*I, *Bsi*WI, *Stu*I, and *Afl*II) were silent. The partly synthetic gene was designated αHL-RL.

The αHL-RL plasmid DNA was then used to create mutant GNN/HQ/H. *Bst*EII and *Stu*I-digested plasmid was ligated to a cassette composed of two phosphorylated oligonucleotides: HB510 (upper strand) GTAACCTTACTGGTAATAATACTCATCAGATTGGAGG, HB511 (lower strand) CCTCCAATCTGATGAGTATTATTACCAGTAGA. Mutant GNN/HQ/H plasmid DNA was then digested with *Avr*II and *Afl*II, and ligated with the following phosphorylated oligonucleotides to create the mutant GNN/HQ/N: HB523 (upper strand) CTAGGTAATACAC, HB524 (lower strand) TTAAGTGTATTAC. Three other mutants were generated using *Bst*EII and *Stu*I-digested GNN/HQ/N plasmid DNA. These mutants and the oligonucleotides that were used to generate them are 1) DNN/HQ/N-HB563 (upper strand) GTAACCTTACTGATAATAATACTCATCAGATTGGAGG, HB566 (lower strand) CCTCCAATCTGATGAGTATTATTATCAGTAAG; 2) GDN/HQ/N-HB564 (upper strand) GTAACCTTACTGGTGATAATACTCATCAGATTGGAGG, HB567 (lower strand)

TABLE 1 A comparison of the primary sequences of wild type and mutant versions of αHL used in this study

	Amino Acid Residues													
αHL Type	8/	124/	126	127	128	129	130	131	132	133	134/	139/	142/	144
Wild type	K	V	G	D	D	T	G	K	I	G	G	N	I	H
K8A	A													
T129H	A					H								
G130H	A						H							
K131H	A							H						
I132H	A								H					
G133H	A									H				
G134H	A										H			
RL	A	L					S					Q	L	
GNN/HQ/H	A	L		N	N		H	Q				Q	L	
GNN/HQ/N	A	L		N	N		H	Q				Q	L	N
DNN/HQ/N	A	L	D	N	N		H	Q				Q	L	N
GDN/HQ/N	A	L		D	N		H	Q				Q	L	N
GND/HQ/N	A	L		N	D		H	Q				Q	L	N

Only the amino acids that were substituted are listed. Amino acid side chains that bind protons and coordinate transition-metal divalent cations are underlined [e.g., His (H), Asp (D), and Lys (K)]. Breaks in the primary sequence are denoted by slashes (/).

CCTCCAATCTGATGAGTATTATCACCAGTAAG; and 3) GND/HQ/N-HB565 (upper strand) GTAACCTTACTGGTAATGATACTCATCAGATT-GGAGG, HB568 (lower strand) CCTCCAATCTGATGAGTATCATTAC-CAGTAAG. Mutations were confirmed by DNA sequencing. No sequence differences were observed in αHL DNA other than those present in the mutagenic oligonucleotides.

Protein purification

WT-αHL from *S. aureus* Wood strain 46 (American Type Culture Collection), recombinant αHL from the αHL negative *S. aureus* strain DU1090 (Fairweather et al., 1983) and recombinant αHL expressed in *Escherichia coli* strain JM109(DE3) (Promega, Madison, WI) were purified as described elsewhere (Cheley et al., 1997; Palmer et al., 1993).

In certain cases, as indicated in the text, mutant αHL polypeptides were synthesized in vitro by coupled transcription and translation (IVTT), as described previously (Walker et al., 1992). Briefly, supercoiled plasmid DNA was used as the template in an *E. coli* S30 extract (Promega, No. L464) supplemented with rifampicin (20 μg/ml) and T7 RNA polymerase (2000 U/ml; New England Biolabs, Beverly, MA). To facilitate the monitoring of the purification, an IVTT reaction (25 μl), carried out in the presence of [^{35}S]methionine (400 μCi/ml, 1200 Ci/mmol; New England Nuclear Life Science Products, Boston, MA) was mixed with an unlabeled IVTT reaction (100 μl). Polyethylenimine (PEI, 10% aqueous solution), prepared as described elsewhere (Gegenheimer, 1990), was added to a final concentration of 0.2% and the mixture was then placed on ice for 10 min. The PEI-treated extract was centrifuged in a microfuge tube at 16,000 × *g* for 10 min at 4°C. A 50% slurry of SP Sephadex C50 cation exchanger (50 μl) that had been equilibrated in 10 mM Tris-HCl (pH 8) was added to the supernatant. After mixing, the suspension was applied to a 2-ml capacity 0.2 μm cellulose acetate microfilterfuge tube (Rainin) and centrifuged for 2 min at 16,000 × *g*. The filtrate was diluted 10-fold in 10 mM sodium acetate (pH 5.2). A 50% slurry of S-Sepharose FF cation exchanger (60 μl) that had been equilibrated with 10 mM sodium acetate (pH 5.2) was then added. The mixture was rotated gently for 1 h at 4°C, placed in another microfilterfuge tube, and centrifuged to remove unbound protein from the resin. The spin filter containing the ion exchange resin was then inserted into a fresh microfilterfuge tube. Bound αHL was eluted from the resin by mixing it with 4 bed volumes of elution buffer (120 μl of 300 mM NaCl in 10 mM sodium acetate, pH 5.2) followed by centrifugation for 2 min. Recovery of the mutant αHL protein was monitored by hemolytic assay (see below) as well as by autoradiography after electrophoresis in a 12% SDS-polyacrylamide gel.

Hemolytic assays in microtiter wells

After translation, the IVTT mix was centrifuged at 16,000 × *g* for 10 min and the supernatant was used immediately. For hemolysis assays in the presence of EDTA or metal ions, 10 μl of IVTT mix was diluted with Na MOPS-BSA (10 mM Na MOPS, 150 mM NaCl, pH 7.4 containing 1 mg/ml bovine serum albumin) buffer (70 μl) and subjected to twofold serial dilution with Na MOPS-BSA buffer (40 μl in each of 12 wells of a 96 well microtiter dish). EDTA (10 μl of 5 mM) or 1 mM metal sulfate (10 μl) was then added to the wells and lysis was measured for 1 h at 20°C after the addition of 1% washed rabbit erythrocytes (50 μl in Na MOPS-BSA) by monitoring the increase in light transmitted at 595 nm using a Bio-Rad microplate reader (Model 3550-UV).

Single channels in planar lipid bilayers

Solvent-free planar lipid bilayer membranes were formed from diphytanoyl phosphatidylcholine (DiPhyPC; Avanti Polar Lipids, Inc., Alabaster, AL), in high purity pentane (Burdick and Jackson, Muskegon, MI) on a 100–150 μm diameter orifice in a 17- or 25-μm-thick Teflon partition that separated two chambers (Montal and Mueller, 1972; Kasianowicz et al., 1996). The orifice was pretreated with a 10% (v/v) solution of purum grade hexadecane (Fluka, Buchs, Switzerland) in pentane.

The aqueous solutions bathing the membrane were prepared with 1 M KCl (Mallinckrodt, St. Louis, MO), 5 mM ultrol grade HEPES (Calbiochem, San Diego, CA), or 5 mM BioChemika micro select grade MOPS (Fluka) in deionized H_2O (Barnstead NANOpure II, Dubuque, Iowa) and titrated to pH 7.5 using 1 N NaOH (Fisher Scientific, Pittsburgh, PA). Trace heavy metal contaminants were subsequently removed by passing the solution through a 1.5-cm diameter glass column containing 10 ml Chelex-100 ion exchange resin (Bio-Rad, Hercules, CA). The bulk conductivity of aqueous solution samples was measured using a Radiometer Model 82 conductivity meter (Copenhagen, Denmark).

Single channels were formed by adding <1 μg of either WT-αHL or mutant-αHL to 1.8 ml of solution in the *cis* chamber while stirring. When a single channel appeared, the chamber was flushed extensively with fresh buffer to eliminate further channel incorporation.

Divalent cations were added to the *cis* or *trans* chambers by adding <20 μl total of concentrated stock solutions of the following reagents, which were used without further purification: zinc sulfate (Matheson, Coleman and Bell, Norwood, OH), cupric sulfate and nickel sulfate (Mallinckrodt, St. Louis, MO), calcium sulfate (Aldrich, Milwaukee, WI) and cobalt chloride (Fisher Scientific, Fairlawn, NJ). Although some of the mutant αHLs had submicromolar binding constants for metal ions, as judged by the effect of Zn(II) on the single channel current, we restricted our study to the effects caused by divalent cations at concentrations between 1 μM and 1 mM. Where noted, excess EDTA (tri-sodium salt, Sigma, St. Louis, MO) titrated to pH 7.5 was added to the chambers to completely chelate the divalent cations. The pH of the solutions in each chamber at the end of an experiment varied by <0.15 from the initial reading, and the temperature was $T = 23.0 \pm 1.5$°C.

The potential difference was applied across the bilayer with Ag-AgCl electrodes in 3 M KCl, 1.5% agarose bridges (Bethesda Research Laboratory, Gaithersburg, MD). The polarity of the potential is defined as positive when it is greater at the side of protein addition (*cis*). The current was converted to voltage and amplified by either a Dagan 3900A (Minneapolis, MN) or an Axopatch 200A (Foster City, CA) patch-clamp amplifier in the whole cell mode with a modified 3902 or a CV-201AU headstage, respectively. The signal was digitized using a SONY/Dagan/Unitrade DAS 75 data recorder onto DAT tape and subsequently transferred to a personal computer through a Frequency Devices model 902 or 9002 8-pole Bessel filter (Haverhill, MA), the corner frequency of which was set to <⅜ of the sampling frequency of a National Instruments AT-MIO-16X A/D board (Austin, TX). The membrane chamber and headstage were isolated from external electrical and magnetic noise sources by a mu-metal box (Amuneal Corp., Philadelphia, PA).

Under certain conditions, the binding of protons and divalent cations to WT-αHL causes it to gate to much lower conductance states (the ratio of the final to the initial conductance is ~0.1) over time scales that range from 100 ms to seconds, depending on the concentration of each analyte and the magnitude of the applied potential (Menestrina, 1986; Korchev et al., 1995, Kasianowicz and Bezrukov, 1995). To avoid these cation-induced gating effects, we used a higher electrolyte concentration (1 M KCl), a relatively low applied potential (−40 mV), relatively low concentrations of Zn(II) ($[ZnSO_4] \leq 1$ mM), and a relatively high pH (pH 7.5), compared to those used previously (e.g., Menestrina, 1986).

RESULTS AND DISCUSSION

Hemolytic assay

We first screened the scanning histidine mutants T129H, G130H, K131H, I132H, G133H, and G134H for pore-forming activity as a function of Zn(II) concentration using the hemolysis assay described above. WT-αHL lyses rabbit red blood cells (rRBCs) by forming large pores in the erythrocyte membrane. As the cells rupture, the light trans-

mitted by the sample increases. In the absence of divalent cations, WT-αHL (*solid circles*) and the point His mutants had closely similar lytic activities (Fig. 1). For visual clarity, the only mutant αHL results that are shown are T129H (*solid diamonds*), G130H (*solid triangles*), and G134H (*solid squares*). Adding 100 μM Zn(II) had no effect on WT-αHL's hemolytic activity (*open circles*), a slight effect on the lytic activity by T129H (*open diamonds*), or K131H (not shown) and a marked inhibitory effect on the lytic activity of G130H (*open triangles*), G134H (*open squares*), I132H (not shown), or G133H (not shown). The results of this experiment suggest that the His-mutants G130H, I132H, G133H, and G134H might be useful as sensing elements for metal ions.

Determining the Zn(II) binding site and structural implications

The hemolytic assay did not allow us to distinguish whether Zn(II) inhibited the assembly of the pore or occluded a fully formed channel. To address that question, and to identify which residues constitute the metal ion binding site, we studied the effects of divalent metal cations on the single-channel currents of one of the point His mutants, G130H, and the last five mutants listed in Table 1 (see above). We show below that by altering the number and location of ionizable side chains in select locations between 126 and 144, we determined the residues that comprise the binding site and confirmed part of the channel's proposed structure (Song et al., 1996).

In the absence of Zn(II), the single channel currents for WT-αHL and each of these mutants were relatively noise free (e.g., see Fig. 3). In the presence of 1 μM Zn(II) in the *trans* compartment, the current carried by potassium and chloride ions through WT-αHL is quiescent (Fig. 2, *leftmost current trace*). However, Zn(II) induced pronounced current fluctuations in three of the five mutant αHLs studied here (Fig. 2, *traces 2–6*).

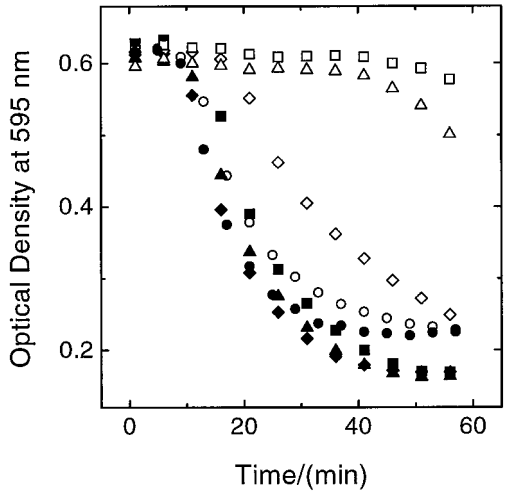

FIGURE 1 Wild-type and histidine point mutants of αHL form lytic pores. Zn(II) inhibits the hemolytic activity of several mutant proteins. The filled and open symbols indicate the absence and presence of Zn(II), respectively. Without Zn(II), WT-αHL (*circles*), T129H (*diamonds*), G130H (*triangles*), and G134H (*squares*) caused 50% lysis of rabbit RBCs within 15 min. Adding Zn(II) had virtually no effect on the hemolytic activity of WT-αHL but inhibited hemolysis by the point histidine mutants to varying degrees. Ionizable side chains are underscored.

The first two recordings show that the single point mutation, Gly replaced by His at position 130 (G130H, i.e., GDD/HK/H), is sufficient to confer Zn(II) sensitivity to the channel. Crystallographic and other evidence suggest that the channel is composed of seven identical αHL monomers (Gouaux et al., 1994; Song et al., 1996). Zn(II) can coordinate four ionizable residues. Therefore, it was conceivable that Zn(II) was coordinated by His-130 side chains on different monomers. The third current trace demonstrates that this conclusion was not correct. Specifically, a mutant αHL with His-130 and with the four ionizable side chains immediately up and downstream of it replaced with non-ionizable counterparts (GNN/HQ/N) showed no Zn(II)-induced current fluctuations. Therefore, the metal binding site consists of His-130 and one (or more) of the four ionizable amino acids that are proximal to that site (i.e., D127, D128, K131, and H144).

Zn(II)-induced current fluctuations reappeared when Asp-128 and His-130 were both present (GND/HQ/N, *fourth trace*). However, the fifth trace shows that the current fluctuations were virtually absent, if instead, the coordinating side chains were Asp-127 and His-130 only (GDN/HQ/N). These two results suggest that the binding site is primarily His-130 and Asp-128. We do not know whether the chelation occurs between these two residues within a monomer or between Asp-128 and His-130 on different monomers.

We determined the channel's structural motif in this segment of the polypeptide with an additional substitution. When the only ionizable side chain proximal to His-130 was Asp-126, the current fluctuations reappeared (DNN/HQ/N, *sixth current trace*). Interestingly, the current noise was even more pronounced than that observed with the other mutants reported here. Because His-130 only coordinates Zn(II) with ionizable side chains at residues 126 or 128, the minimum interval defining a binding site is two residues, not four. This suggests the secondary structure of the channel in this region is β-sheet and not α-helix (Arnold and Haymore, 1991). This conclusion is consistent with the crystal structure of WT-αHL oligomerized in detergent (Song et al., 1996).

Note that the Zn(II)-induced current blockades for the point mutants G130H and GND/HN/N (Fig. 2, *second* and *fourth traces*, respectively) were qualitatively different, which suggests the metal binding site is not completely defined by His-130 and Asp-128. Thus, one or more of the ionizable side chains Asp-127, Lys-131, or His-144 might play a minor role in determining the geometry and/or electrostatics of the M(II) coordination, but probably do not directly participate in the metal ion binding activity reported

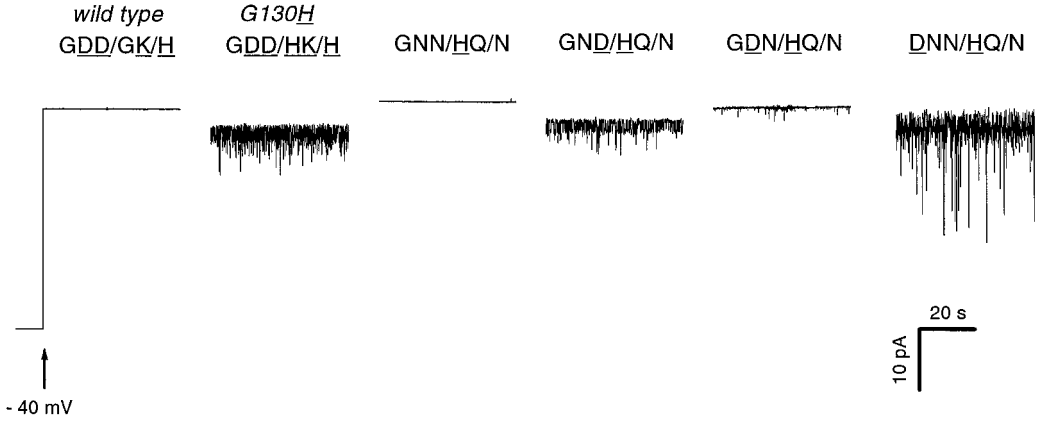

FIGURE 2 Single channel recordings of genetically engineered αHL mutants define the Zn(II) binding site and part of the channel structure in planar lipid bilayers. The side chains of amino acids at sites 126, 127, 128, 130, 131, and 144 are listed above the recordings, and the Zn(II) concentration in the *trans* chamber was 1 μM. See text for details.

here. This conclusion is justified experimentally for Asp-127 because it caused virtually no Zn(II)-induced current fluctuations (Fig. 2, *fifth trace*). His-144 is too far from His-130 to coordinate Zn(II) (Song et al., 1996).

At first glance, it might seem remarkable that Zn(II) can be chelated by Asp-126 and His-130 (Fig. 2, *rightmost trace*) because of the large distance that would separate the two side chains if they were within the same continuous segment of a β-sheet. This result suggests that these two side chains lie adjacent to each other on opposite sides of a reverse turn in the β-sheet. That conclusion is consistent with the crystal structure of the heptamer, which identifies T129 as the locus of the β-sheet turn at one entrance of the pore (Song et al. 1996).

The crystal structure of WT-αHL also predicts that amino acid side chains at positions 126 and 130 would point outside of the water-filled pore (Song et al., 1996). However, that structure cannot predict whether these residues are located in the hydrophobic milieu of the membrane or in the aqueous phase outside the channel's lumen. Because the energy barrier for divalent cations to partition into a lipid bilayer membrane is formidable (Parsegian, 1969), the accessibility of the side chains Asp-126 and His-130 to Zn(II) suggests that they are both in the aqueous phase and not buried in the hydrophobic part of the membrane. Measurements of the spectral response of a polarity-sensitive fluorescent dye attached to point Cys αHL mutants (Valeva et al., 1996) suggested that side chain 126 is located in the membrane when the protein is reconstituted into liposomes. This is contrary to what we conclude here for single αHL channels formed in DiPhyPC planar bilayer membranes and may be due to a difference in how αHL is situated in the two membrane systems or because the fluorophore is large and therefore capable of extending into the bilayer. It is also interesting that current blockades were induced by Zn(II) coordinated to side chains located on the outside of the channel. We return to this point later.

Effect of Zn(II) on single channel currents of WT-αHL and GND/HQ/N

The effect of 1 μM to 1 mM Zn(II) (*trans*) on the single channel current of WT-αHL and that of the mutant in which the metal binding site is defined by Asp-128 and His-130 (GND/HQ/N) is shown in Fig. 3 (the mean current was subtracted from each recording). Concentrations of Zn(II) ≤ 1 mM had no effect on the WT-αHL single channel current (*left column of current traces*). In contrast, 1 μM Zn(II)

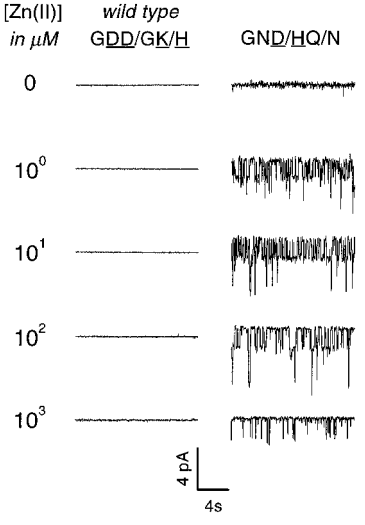

FIGURE 3 [Zn(II)] ≤ 1 mM had no effect on WT-αHL but induced concentration-dependent current fluctuations in GND/HQ/N. The recordings show that Zn(II) induced single channel current fluctuations by binding to a coordination site defined by Asp-128 and His-130. When the [Zn(II)] was increased, the fluctuations in the current through the mutant channel reached a maximum (at [Zn(II)] = 10 μM) and then decreased. Although the channel is formed by seven identical monomers, only three well-defined conductance states were observed with this mutant. The mean current was subtracted from all recordings. $ZnSO_4$ was added to the *trans* compartment only and a −40 mV potential was applied across the membrane. The data were acquired at 100 Hz and filtered at 10 Hz.

caused well-defined current blockades in GND/HQ/N and the current fluctuations became less prevalent as the divalent cation concentration was increased beyond 10 μM (*right column of current traces*). This result can be qualitatively described by assuming that Zn(II) complexes reversibly with each metal-ion binding site on the channel formed by GND/HQ/N. Higher concentrations of Zn(II) saturate the binding sites, which causes the current fluctuations to occur less frequently. This effect is similar to the fluctuations in current caused by the reversible binding of hydrogen or deuterium ions to ionizable residues in the WT-αHL channel (Bezrukov and Kasianowicz, 1993; Kasianowicz and Bezrukov, 1995). However, the analogy is not completely identical because the kinetics of the protonation reactions are more rapid compared to those of Zn(II) binding to sites on these mutant channels and because the binding of protons to WT-αHL causes the current to increase.

Because the channel is a heptamer formed from identical monomers (Gouaux et al., 1994; Song et al., 1996) and at least two ionizable residues per monomer define the binding site, there could be seven or more distinct metal binding sites per channel. The current recordings in Fig. 3 show that in the presence of Zn(II), there were predominately three distinct conductance states in the channel formed by GND/HQ/N. Higher bandwidth recordings (f_c = 1 kHz) showed that in the presence of 1 to 10 μM Zn(II), there were at least four distinct conductance states in this channel or with that formed by G130H (data not shown). Thus, only three Zn(II) binding sites per channel were readily apparent. Because the sites are in close proximity, the probability that an individual metal binding site is occupied by Zn(II) could be altered by the state of Zn(II) occupancy of the neighboring sites. A similar conclusion was drawn for hydrogen (Bezrukov and Kasianowicz, 1993, Kasianowicz and Bezrakov, 1995) and deuterium ions (Kasianowicz and Bezrukov, 1995) binding to the WT-αHL channel. However, in those studies, it was not possible to directly observe conductance changes caused by the binding of single protons to the channel. Instead, the number of these sites ($N = 4$) was deduced from the H^+- or D^+-induced current noise assuming that the sites had identical *pKs* and the binding of each proton contributes equally to the total difference in conductance at the extremes of pH.

Location of the Zn(II) binding site

To confirm at which end of the pore the binding site was located, we compared the single channel current blockades caused by Zn(II) added to the *cis* or *trans* compartments. Approximately 50- to 100-fold less Zn(II) *trans* elicited the same effect on the single channel current of GND/HQ/N for a given concentration of Zn(II) *cis* (data not shown). As we showed above, the turn in the β-sheet is between side chains 126 and 130. We therefore conclude that the residues between 126–130 are located adjacent to the *trans* mouth of the αHL channel. A similar conclusion was drawn for a Cys mutation of αHL at position 130 (Krasilnikov et al., 1997) and is also consistent with the αHL crystal structure (Song et al., 1996).

In addition, if all seven engineered heavy metal binding sites were inside the lumen, we would expect that Zn(II) would reduce the channel conductance to a greater extent than that shown in Fig. 3. The relatively subtle effect at high concentrations of Zn(II) is another indication that the sites located are external to the pore.

Divalent cation specificity of the G130H channel

Metal-induced current fluctuations for single channels formed by G130H depend on the type of divalent cation added to the *trans* chamber (Fig. 4). For example, 100 μM Zn(II) *trans* causes many rapid blocking events per unit time and a distinctive kinetic pattern unlike those caused by the other divalent cations (e.g., Cu(II), Ni(II), or Co(II)) at this concentration. The binding constants for these metal ions follow the sequence Zn(II) > Cu(II) > Ni(II) > Co(II) (data not shown). Ca(II) was virtually ineffective at causing channel blockades, even at 1 mM (data not shown). The current fluctuations induced by divalent cations are completely reversible and are abolished by subsequently adding excess EDTA to the *trans* chamber (data not shown).

Relation of single channel current blockades to Zn(II)-induced inhibition of hemolytic activity

In the absence of Zn(II), the mean single channel current of the pore formed by G130H (GDD/HK/H) was ~33 pA at −40 mV (Fig. 2, *second trace*). Most of the relatively long-lived Zn(II)-induced current blockades at any Zn(II) concentration decreased the current by <15% or 5 pA (Fig. 4, G130H, 100 μM Zn(II) *trans*). Thus, the Zn(II)-induced

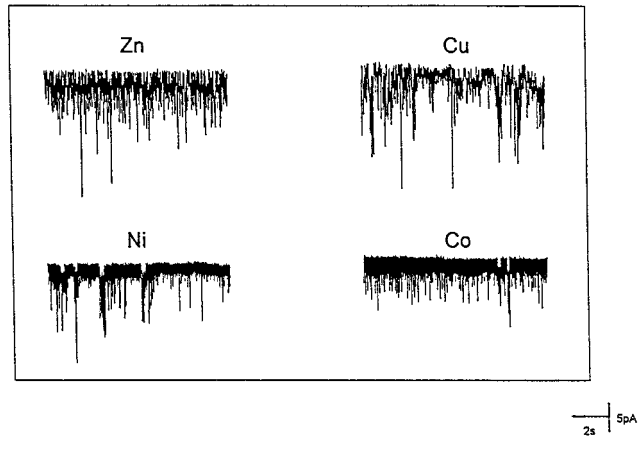

FIGURE 4 The point mutant G130H formed pores with divalent cation specificity. Different divalent cations induced distinct current blockade kinetic patterns in a single G130H channel. The solution on the *trans* side contained 100 μM of either $ZnSO_4$, $CuSO_4$, $NiCl_2$, or $CoCl_2$. The recordings are arranged in order of decreasing blockade frequency (Zn(II), Cu(II), Ni(II), and Co(II)). The data were acquired at 3000 points/s and filtered at 1 kHz.

inhibition of this mutant's hemolytic activity (Fig. 1, *open triangles*) might be caused by a block in channel assembly in rRBC membranes rather than by the occlusion of preformed pores. The latter mechanism of hemolysis inhibition was dominant for the mutant H5-αHL in which the five amino acid residues between 130–134 (GKIGG) were each replaced by His (Walker et al., 1994).

On the use of scanning mutagenesis and conductance measurements to locate residues in a channel's pore

The three-dimensional crystallographic structures of most membrane-bound proteins are unknown. Thus, alternative methods to deduce their structure and function have been developed. For example, site-specific mutagenesis combined with nitroxide spin labeling of those sites allowed the assignment of secondary structure motifs to specific regions in bacteriorhodopsin (Altenbach et al., 1990), colicin E1 (Todd et al., 1989), and in voltage-gated channel-forming peptides (Barranger-Mathys and Cafiso, 1996).

Because ionic channels have the unique property of having their functional pathway available for interrogation by ionic conductance measurements, scanning mutagenesis studies are also performed to determine which amino acid side chains line the channel lumen. Side chains that bind or react with a chemical reagent are substituted into the channel's primary structure. If the mutant channel's conductance is altered by the reagent, it is assumed that the amino acid that contains the binding site lines the channel's lumen. Cysteine scanning mutagenesis was used to identify sites in the lumens of several channels (e.g., Backx et al., 1992; Akabas et al. 1992; Akabas and Karlin, 1992; Ramirez-Latorre et al., 1996). In this study we showed that 1 μM Zn(II) caused current fluctuations when the metal binding site was defined by either Asp-128 and His-130 (GN<u>D</u>/<u>H</u>Q/N) or Asp-126 and His-130 (<u>D</u>NN/<u>H</u>Q/N) (Fig. 2). In the absence of other structural information, it would be tempting to conclude that these side chains are, in fact, inside the pore. However, the crystal structure of WT-αHL locates Gly-126, Asp-128, and Gly-130 *outside* the channel lumen, near the *trans* chamber mouth (Song et al., 1996). Thus, the divalent cation-induced conductance fluctuations reported here might not be caused by blockades of the channel lumen. Instead, they may be the result of Zn(II)-induced alterations in either the channel's structure or the electrostatic potential that drives ions through the channel.

It is also conceivable that the channel's structure is sufficiently flexible in this region to allow the residues 126, 128, and 130 to occasionally lie in the pore. Although we cannot rule that out at this time, previous work with fluorescent probes suggest this is possible (Valeva et al., 1997). Nevertheless, we have demonstrated here that analyte-induced conductance fluctuations are not a sufficient condition to conclude that a coordinating or reactive side chain is always inside a channel's lumen.

The need for a more cautious interpretation of the physical cause of analyte-induced current changes is made even more apparent by the effects of Zn(II) on the single channel current of mutant <u>D</u>NN/<u>H</u>Q/N. At low Zn(II) concentrations, transient current blockades were evident (Fig. 5, *top*). As the Zn(II) concentration was increased the current blockades became less apparent. However, Zn(II) altered the mean current in a surprising manner. Specifically, the Zn(II)-induced current blockades slightly decreased the mean current at 1 μM Zn(II) (*bottom*). However, the mean current actually increased with increasing Zn(II) concentration above 1 μM (*both panels*). Similar results were obtained at +40 mV (data not shown). While we do not know the physical causes underlying these two contrasting effects, the 12% increase in the mean current was not due to the negligible ($< 0.2\%$) increase in the bulk solution conductivity caused by 1 mM $ZnSO_4$.

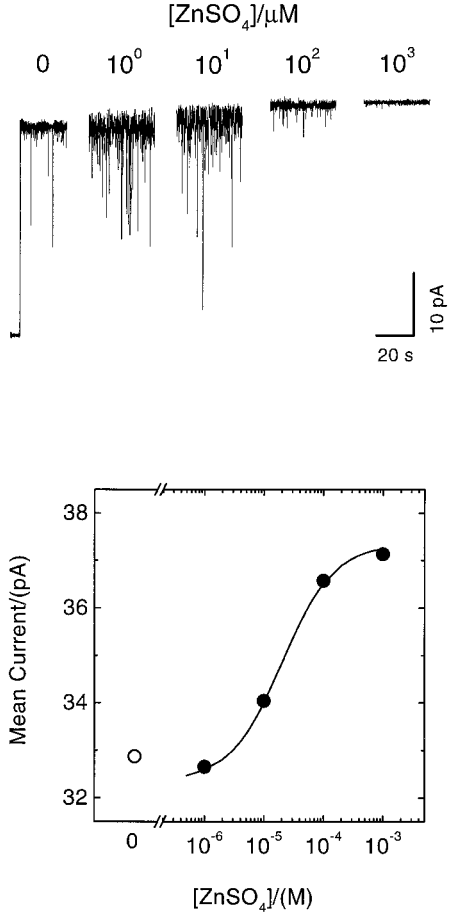

FIGURE 5 Zn(II) had two opposing effects on the single channel current of a channel with a chelation site defined by Asp-126 and His-130 (<u>D</u>NN/<u>H</u>Q/N). *Top panel:* Increasing the concentration of $ZnSO_4$ (*trans*) caused marked transient increases and decreases in the current. As the Zn(II) concentration increased, the current fluctuations disappeared and the mean current increased compared to that in the absence of Zn(II). *Bottom panel:* The dependence of the mean current on the $ZnSO_4$ concentration. The solid line through the points illustrates the result of a least squares fit to a single binding constant model (K = 18 μM) to the data. Upon transfer to the computer, the current was filtered at 10 Hz and oversampled at 100 Hz. The applied potential was −40 mV.

It is also interesting to compare the effects of other charged analytes (e.g., protons) on different channels. The currents through some Ca^{2+} channels are blocked by protons (Pietrobon et al., 1988; Prod'hom et al., 1987; Root and MacKinnon, 1994; Chen et al., 1996) whereas the binding of protons to WT-αHL causes the current to increase (Bezrukov and Kasianowicz, 1993; Kasianowicz and Bezrukov, 1995). In all of these studies it was concluded that the proton binding sites for each of these channels were inside the pore. Our results suggest that these conclusions, and those based on the results of scanning mutagenesis, warrant further consideration.

Summary

The crystal structure of WT-αHL locates residues 126, 128, and 130 on the outside surface of the pore's β-barrel. A representation of the channel's structure, which highlights only one of the seven anti-parallel β-sheets that form the pore, is shown in Fig. 6. The experimental evidence shown here corroborates part of the pore's β-sheet motif and the location of the turn at the *trans* channel mouth. It also suggests that the *trans* membrane surface is located above side chain 126 and that channel blockades can occur even when the binding site is located outside a channel's lumen.

Future goals

In addition to corroborating structural information about the αHL ion channel, we are using scanning histidine mutagenesis to assess αHL's ability to function as a biosensor component. One of our long-range objectives is to design and produce ion channels with different sensitivities to, and specificities for, a variety of water-soluble analytes. To accomplish this goal, we are constructing stable ion channels with well-defined binding sites associated with the pore to which an analyte of choice can couple. The results in Figs. 1–5 show that simple modifications to αHL induced Zn(II) sensitivity to this channel. Fig. 4 demonstrates that genetic engineering can also be used to confer some degree of analyte specificity to it as well. Although highly desirable, it is not an absolute requirement that a sensor possess perfect selectivity. Spectral methods (Stevens, 1977; DeFelice, 1981; Kasianowicz et al., 1994; Kasianowicz and Bezrukov, 1995) combined with an estimate of the single channel current should prove useful in distinguishing between two different ions in solution, because the rate constants for the reactions will be characteristic of each ion species that binds to the site. In principle, the relative contribution of several analytes competing for the same binding sites should be accessible to spectral decomposition as well.

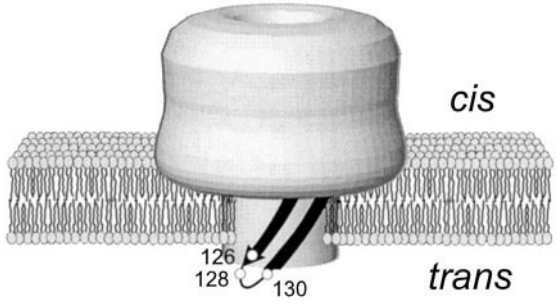

FIGURE 6 A representation of the α-hemolysin ion channel's crystal structure. Only one of the seven antiparallel β-sheet pairs, which comprise the pore, is shown. The results of this study corroborate the pore's structure adjacent to the *trans* entrance.

Cornell et al. (1997) recently reconstituted an ion channel "switch" into rugged supported bilayer membranes. By using impedance spectroscopy they showed that the channel-forming activity of gramicidin was altered by the presence of the analyte, which either released inactive peptide from anchorage sites or sequestered it there.

We note here that genetically engineered pores might also prove useful in other applications, including the characterization and separation of charged and neutral polymers. For example, the WT-αHL channel was used to determine some of the physical properties of polynucleotides. Specifically, an applied electric field forced RNA and DNA to traverse the WT-αHL channel, giving rise to ionic current blockades with characteristic lifetimes that were proportional to the polynucleotide length (Kasianowicz et al., 1996).

We thank Renee Li for technical assistance in some of the experiments and Sean Lee for writing some of the computer programs used in the data acquisition.

This work was supported in part by a National Academy of Sciences/National Research Council Research Associateship (to J.J.K.), a National Science Foundation graduate student fellowship (to D.B.), and by grants from the Office of Naval Research and the Department of Energy (to H.B.). Commercial names of materials and apparatus are identified only to specify the experimental procedure. This does not imply a recommendation by NIST, nor does it imply that they are the best available for the purpose.

REFERENCES

Akabas, M. H., and A. Karlin. 1992. Identification of acetylcholine receptor channel-lining residues in the M1 segment of the α-subunit. *Biochemistry*. 34:12496–12500.

Akabas, M. H., D. A. Stauffer, M. Xu, and A. Karlin. 1992. Acetylcholine receptor channel structure probed in cysteine-substitution mutants. *Science*. 258:307–310.

Altenbach, C., T. Marti, H. G. Khorana, and W. L. Hubbell. 1990. Transmembrane protein structure: spin labeling of bacteriorhodopsin mutants. *Science*. 248:1088–1092.

Arnold, F. H., and B. L. Haymore. 1991. Engineered metal-binding proteins: purification to protein folding. *Science*. 252:1796–1797.

Backx, P. H., D. T. Yue, J. H. Lawrence, E. Marban, and G. Tomaselli. 1992. Molecular localization of an ion-binding site within the pore of mammalian sodium channels. *Science*. 257:248–251.

Barranger-Mathys, M., and D. S. Cafiso. 1996. Membrane structure of voltage-gated channel forming peptides by site-directed spin-labeling. *Biochemistry*. 35:498–505.

Bezrukov, S. M., and J. J. Kasianowicz. 1993. Current noise reveals protonation kinetics and number of ionizable sites in an open protein ion channel. *Phys. Rev. Lett.* 70:2352–2355.

Bezrukov, S. M., and J. J. Kasianowicz. 1997. Charge state of an ion channel controls neutral polymer entry into its pore. *Eur. Biophys. J.* 6:471–476.

Bezrukov, S. M., I. Vodyanoy, R. A. Brutyan, and J. J. Kasianowicz. 1996. Dynamics and free energy of polymers partitioning into a nanoscale pore. *Macromolecules*. 29:8517–8522.

Braha, O., B. Walker, S. Cheley, J. J. Kasianowicz, L. Song, J. E. Gouaux, and H. Bayley. 1997. Designed protein pores as components for biosensors. *Chem. Biol.* 4:497–505.

Cheley, S., M. S. Malghani, L. Song, M. Hobaugh, J. E. Gouaux, J. Yang, and H. Bayley. 1997. Spontaneous oligomerization of a staphylococcal α-hemolysin conformationally constrained by removal of residues that form the transmembrane β-barrel. *Protein Eng.* 10:1433–1443.

Chen, X.-H., I. Bezprozvanny, and R. W. Tsien. 1996. Molecular basis of proton block of L-type Ca^{2+} channels. *J. Gen Physiol.* 108:363–374.

Cornell, B. A., V. L. B. Braach-Maksvytis, L. G. King, P. D. J. Osman, B. Raguse, L. Wieczorek, and R. J. Pace. 1997. A biosensor that uses ion-channel switches. *Nature (Lond.)*. 387:580–583.

DeFelice, L. J. 1981. An Introduction to Membrane Noise. Springer Verlag, New York.

Fairweather, N., S. Kennedy, T. J. Foster, M. Kehoe, and G. Dougan. 1983. Expression of a cloned *Staphylococcus aureus* α-hemolysin determinant in *Bacillus subtilis* and *Staphylococcus aureus. Infect. Immun.* 41: 1112–1117.

Gegenheimer, P. 1990. Guide to protein purification. *In:* Methods in Enzymology, Vol. 182. M. P. Deutcher, editor. Academic Press, New York. 193.

Gouaux, J. E., O. Braha, M. R. Hobaugh, L. Song, S. Cheley, C. Shustak, and H. Bayley. 1994. Subunit stoichiometry of staphylococcal α-hemolysin in crystals and on membranes: a heptameric transmembrane pore. *Proc. Natl. Acad. Sci. USA.* 91:12828–12831.

Gray, G. S., and M. Kehoe. 1984. Primary sequence of the α-toxin gene from *Staphylococcus aureus* Wood 46. *Infect. Immun.* 46:615–618.

Hille, B. 1992. Ionic Channels of Excitable Membranes, 2nd ed. Sinauer Assoc., Sunderland, MA.

Kasianowicz, J. J., and S. M. Bezrukov. 1995. Protonation dynamics of the α-toxin channel from spectral analysis of pH dependent current fluctuations. *Biophys. J.* 69:94–105.

Kasianowicz, J. J., E. Brandin, D. Branton, and D. W. Deamer. 1996. Characterization of individual polynucleotide molecules using a membrane channel. *Proc. Natl. Acad. Sci. USA.* 93:13770–13773.

Kasianowicz, J., B. Walker, M. Krishnasastry, and H. Bayley. 1994. Genetically engineered pores as metal ion biosensors. *MRS Symp*. 330: 217–223.

Korchev, Y. E., C. L. Bashford, G. M. Alder, J. J. Kasianowicz, and C. A. Pasternak. 1995. Low conductance states of a single channel are not 'closed'. *J. Membr. Biol.* 147:233–239.

Krasilnikov, O., M.-F. P. Capistrano, L. N. Yuldasheva, and R. A. Nogueira. 1997. Influence of Cys-130 *S. aureus* alpha-toxin on planar bilayer and erythrocyte membranes. *J. Membr. Biol.* 156:157–172.

Krasilnikov, O., R. Z. Sabirov, V. I. Ternovsky, P. G. Merzliak, and J. N. Murathojaev. 1992. A simple method for the determination of the pore radius of ion channels in planar lipid bilayer membranes. *FEMS Microbiol. Immunol.* 105:93–100.

Kunkel, T. A. 1985. Rapid and efficient site-specific mutagenesis without phenotypic selection. *Proc. Natl. Acad. Sci. USA.* 82:488–492.

Menestrina, G. 1986. Ionic channels formed by *Staphylococcus aureus* alpha-toxin: voltage-dependent inhibition by divalent and trivalent cations. *J. Membr. Biol.* 90:177–190.

Montal, M., and P. Mueller. 1972. Formation of bimolecular membranes from lipid monolayers and study of their properties. *Proc. Natl. Acad. Sci. USA.* 65:3561–3566.

Palmer, M., R. Jursch, U. Weller, A. Valeva, K. Hilgert, M. Kehoe, and S. Bhakdi. 1993. *Staphylococcus aureus* α-toxin. Production of functionally intact, site-specifically modifiable protein by introduction of cysteine at positions 69, 130, and 186. *J. Biol. Chem.* 268:11959–11962.

Parsegian, V. A. 1969. Energy of an ion crossing a low dielectric membrane. Solution to four relevant electrostatic problems. *Nature (Lond.)*. 221:844–846.

Pietrobon, D., B. Prod'hom, and P. Hess. 1988. Conformational changes associated with ion permeation in L-type calcium channels. *Nature (Lond.)*. 333:373–376.

Prod'hom, B., D. Pietrobon, and P. Hess. 1987. Direct measurements of proton transfer rates to a group controlling the dihydropyridine-sensitive Ca^{2+} channel. *Nature (Lond.)*. 329:243–246.

Ramirez-Latorre, J., C. R. Yu, X. Qu, F. Perin, A. Karlin, and L. Role. 1996. Functional contributions of α5 subunit to neuronal acetylcholine receptor channels. *Nature (Lond.)*. 380:347–351.

Root, M. J., and R. MacKinnon. 1994. Two identical noninteracting sites in an ion channel revealed by proton transfer. *Science*. 265:1852–1856.

Song, L., M. R. Hobaugh, C. Shustak, S. Cheley, H. Bayley, and J. E. Gouaux. 1996. Structure of Staphylococcal α-hemolysin, a heptameric transmembrane pore. *Science*. 274:1859–1866.

Stevens, C. F. 1977. Study of membrane permeability changes by fluctuation analysis. *Nature (Lond.)*. 270:391–396.

Todd, A. P., J. Cong, F. Levinthal, C. Levinthal, and W. L. Hubbell. 1989. Site-directed mutagenesis of colicin-E1 provides specific attachment for spin labels whose spectra are sensitive to local conformation. *Proteins*. 6:294–305.

Valeva, A., I. Walev, M. Pinkernell, B. Walker, H. Bayley, M. Palmer, and S. Bhakdi. 1997. Transmembrane β-barrel of staphylococcal α-toxin forms in sensitive but not in resistant cells. *Proc. Natl. Acad. Sci. USA.* 94:11607–11611.

Valeva, A., A. Weisser, B. Walker, M. Kehoe, H. Bayley, and S. Bhakdi. 1996. Molecular architecture of a toxin pore: a 15-residue-sequence lines the transmembrane channel of staphylococcal alpha-toxin. *EMBO J.* 15:1857–1864.

Walker, B., M. Krishnasastry, L. Zorn, J. Kasianowicz, and H. Bayley. 1992. Functional expression of the α-hemolysin of *Staphylococcus aureus* in intact *Escherichia coli* and in cell lysates. *J. Biol. Chem.* 267:10902–10909.

Walker, B., J. Kasianowicz, M. Krishnasastry, and H. Bayley. 1994. A pore-forming protein with a metal-actuated switch. *Protein Eng.* 7:655–662.